Chemical Science

ROYAL SOCIETY OF CHEMISTRY

EDGE ARTICLE

View Article Online
View Journal | View Issue

Cite this: *Chem. Sci.*, 2024, **15**, 18549

All publication charges for this article have been paid for by the Royal Society of Chemistry

Received 22nd August 2024
Accepted 6th October 2024

DOI: 10.1039/d4sc05640j

rsc.li/chemical-science

Fully tricoordinated assembly unveils a pioneering nonlinear optical crystal $(SbTeO_3)(NO_3)$†

Bo Zhang,[ab] Chun-Li Hu,[ab] Jiang-Gao Mao [ab] and Fang Kong *[ab]

Balancing the critical property requirements is key to surmounting the obstacles in the application of nonlinear optical (NLO) crystals. Tricoordinated units, characterized by nearly the lowest coordination number, are common in inorganic NLO-active oxides; however, crystals solely composed of such units are rare. Herein, by assembling three distinct tricoordinated units (SbO_3, TeO_3, and NO_3) into a single crystal, a pioneering fully tricoordinated NLO material, $(SbTeO_3)(NO_3)$, was synthesized *via* a facile volatilization method. As the first reported tellurite-antimonite NLO crystal, $(SbTeO_3)(NO_3)$ exhibits well-balanced properties: a strong phase-matched second-harmonic generation (SHG) effect (2.2 × KDP), short UV cutoff edge (253 nm) and moderate birefringence (0.081@546 nm). Unlike most deliquescent nitrates, $(SbTeO_3)(NO_3)$ demonstrates exceptional water resistance (>30 days), attributed to its unique hydrophobic layers and stereochemically active lone pair (SCALP) electrons in the Sb^{3+} and Te^{4+} cations. Theoretical calculations reveal that the optical bandgap and SHG effect of $(SbTeO_3)(NO_3)$ are collectively governed by the three tricoordinated motifs, with individual SHG contributions of 20.92%, 23.88%, and 55.12% from $[SbO_3]$, $[TeO_3]$ and $[NO_3]$, respectively. This breakthrough underscores the efficacy of the fully tricoordinated assembly strategy in engineering NLO materials with optimally balanced properties.

Introduction

Nonlinear optical (NLO) materials have played a crucial role in extending the limited wavelength range of lasers through the process of second-harmonic generation (SHG), with significant applications in advanced optoelectronic devices.[1–5] However, a high-quality NLO crystal must satisfy the following rigorous requirements: (i) a pronounced second-order NLO coefficient ($d_{ij} > 0.39$ pm V^{-1}); (ii) a large optical bandgap ($E_g > 4.2$ eV for UV NLO crystals); (iii) a moderate birefringence ($0.05 < \Delta n < 0.1$); and (iv) good physical and chemical stability.[6,7] Furthermore, some of the conditions exhibit negative correlation, such as bandgap and NLO coefficient.[8–11] Therefore, the design and synthesis of new NLO crystals with excellent balanced performance are challenging.[12,13]

It is known that tricoordinated groups, with almost the lowest coordination number among common anionic units, play a unique role in the creation of new SHG crystals. A large number of reported SHG materials contain at least one tricoordinated anionic group.[14–19] From the perspective of the coordination configuration, such tricoordinated groups can be divided into two types: (i) trigonal planar, such as $[BO_3]$, $[NO_3]$, and $[CO_3]$, and (ii) triangular pyramidal, such as $[IO_3]$, $[TeO_3]$, and $[SbO_3]$. The planar trigonal groups typically exhibit a large bandgap and a relatively small SHG coefficient,[20–22] whereas the triangular pyramidal groups show the opposite trend, with a large SHG coefficient and a small bandgap.[23–27] Therefore, they are the ideal functional units to overcome the intrinsic conflict between large bandgap and high SHG intensity. Some new SHG materials with excellent integrated properties have been created by the combination of the two types of tricoordinated groups, such as $Be_2(BO_3)(IO_3)$ (7.2 × KDP, 4.32 eV),[28] $PbCdF(SeO_3)(NO_3)$ (2.6 × KDP, 4.42 eV),[29] and $Pb_2(BO_3)(NO_3)$ (9.0 × KDP, 3.65 eV).[30]

However, most of the mixed-tricoordinated compounds contain other coordination geometry, which may weaken the effect of the tricoordinated groups.[23,31] Therefore, we intended to build a fully tricoordinated structure to eliminate such impacts. To seek the right balance in bandgap and SHG intensity, both trigonal planar and triangular pyramidal groups must be included. We started with simple ternary compounds containing two types of tricoordinated groups only. However, the syntheses of such compounds failed. Full tricoordination is

[a]*State Key Laboratory of Structural Chemistry, Fujian Institute of Research on the Structure of Matter, Chinese Academy of Sciences, Fuzhou 350002, P. R. China. E-mail: kongfang@fjirsm.ac.cn*

[b]*University of Chinese Academy of Sciences, Beijing 100049, P. R. China*

† Electronic supplementary information (ESI) available: Experimental section, computational method, EDS, SEM images and elemental distribution maps, $[Sb_3Te_3]$ 6-MPRs, the 3D structure, TG analysis, PXRD patterns above 1000 °C, structural comparison, crystal data, fractional atomic coordinates and equivalent isotropic displacement parameters, important bond lengths, angles and bond valences, the dipole moments calculation, a summary of reported tellurite nitrate, antimony nitrate and antimony tellurite families and state energies of the H-VB and L-CB of $(SbTeO_3)(NO_3)$. For ESI and crystallographic data in CIF or other electronic format see DOI: https://doi.org/10.1039/d4sc05640j

not the optimal option in these structures, such as $Se_2(B_2O_7)$ (SeO_3 + BO_4)[32] and SbB_3O_6 (SbO_4 + BO_3 + BO_4).[31] Therefore, we decided to explore complex quaternary compounds, which contain three different tricoordinated groups. To enable the three groups to coexist within a single structural type, we planned to select anionic groups with different charges to prevent the competition between bonds with the same electrostatic bond strength.

Our efforts in the development of new SHG materials with fully tricoordinated groups resulted in a novel polar structure, $(SbTeO_3)(NO_3)$, which is composed of $[Sb^{III}O_3]^{3-}$, $[Te^{IV}O_3]^{2-}$ and $[N^{V}O_3]^{-}$ groups (Fig. 1).

Due to the coexistence of trigonal planar $[NO_3]$ and triangular pyramidal $[SbO_3]$ and $[TeO_3]$ groups, $(SbTeO_3)(NO_3)$ demonstrates a strong phase-matched SHG intensity (2.2 × KDP), a short UV cutoff edge (253 nm), a large bandgap (4.32 eV) and a moderate birefringence (0.081@546 nm). Furthermore, in contrast to most nitrates, which are easily deliquescent, $(SbTeO_3)(NO_3)$ can exhibit exceptional water resistance (>30 days) and good growth characteristics with the majority of the crystals exceeding 4 mm in length. Theoretical calculations revealed that the SHG contributions for $[SbO_3]$, $[TeO_3]$ and $[NO_3]$ groups are 20.92%, 23.88%, and 55.12%, respectively, confirming the synergistic effect of these three tricoordinated groups. This work not only provides an excellent candidate for UV SHG materials with well-balanced properties but also validates the feasibility of the fully tricoordinated assembly strategy. Next, we will report on the material's synthesis, structure, and optical properties.

Results and discussion

Colourless rod-like crystals of $(SbTeO_3)(NO_3)$ were successfully synthesized through a solvent evaporation reaction (Fig. 2a). By extending the reaction time and modifying the ratio of reactants, large single crystals with a length exceeding 4 mm can be acquired in substantial quantities. The yield of the crystals reaches 72% based on Te. Energy-dispersive X-ray spectroscopy (EDS) elemental analysis confirmed the presence of Sb, Te, N, and O elements, with an average molar ratio of Sb : Te close to 1.0 : 1.0 (Fig. S1 and S2†). The purity has been verified by powder X-ray diffraction (PXRD) (Fig. 2d).

$(SbTeO_3)(NO_3)$ crystallizes in the orthorhombic space group $Pca2_1$ (Table S1†). Its asymmetric unit encompasses one Sb, one Te, one N and six O atoms located at general sites (Table S2†). As depicted in Fig. 1a, all the cations, Sb^{3+}, Te^{4+} and N^{5+}, are tricoordinated with three oxygen atoms. The lone pair cations, Sb^{3+} and Te^{4+}, form triangular pyramids while the N atom forms a trigonal planar unit. Although $[SbO_3]$ and $[TeO_3]$ feature the same coordination geometry, their bond lengths and angles are different. The Sb–O bond lengths (1.992(4) to 1.999(2) Å) are about 0.08 Å longer than those of Te–O (1.885(4)–1.922(4) Å),

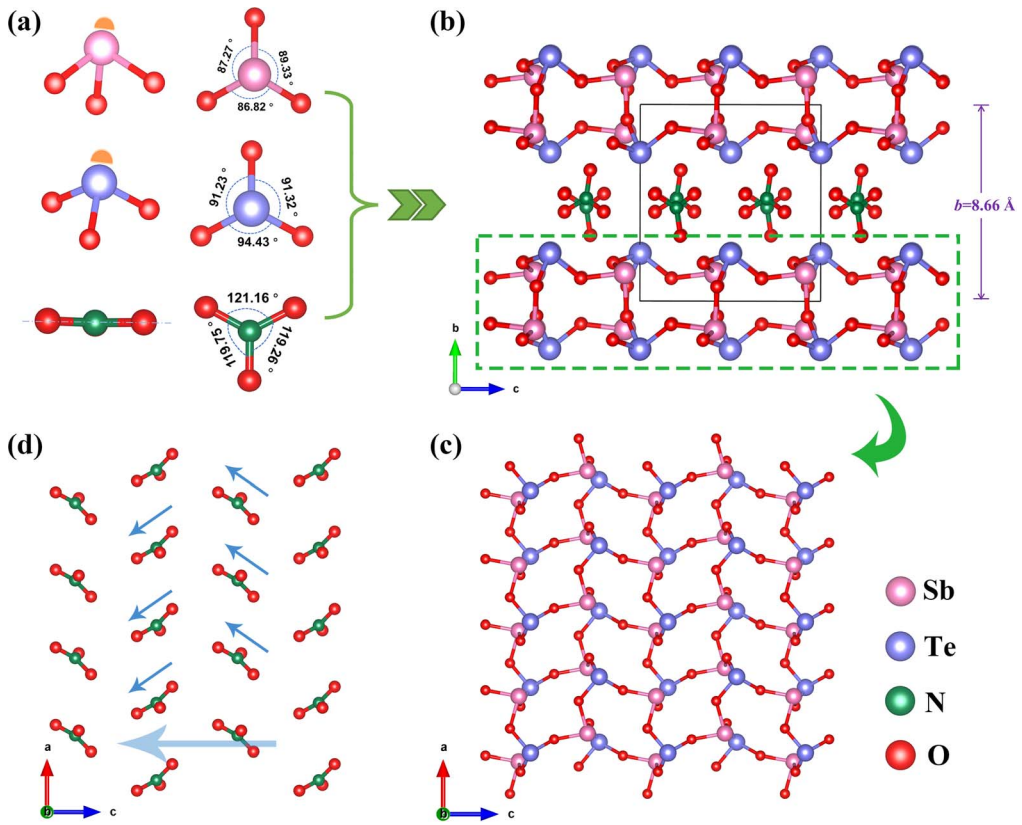

Fig. 1 Tricoordinated $[SbO_3]$, $[TeO_3]$, and $[NO_3]$ fundamental building blocks (a), the sandwich-type 2D layered structure of $(SbTeO_3)(NO_3)$ (b), the 2D $[SbTeO_3]^+$ cationic layer in the *ac* plane (c), and the arrangement of $[NO_3]$ in $(SbTeO_3)(NO_3)$ (d).

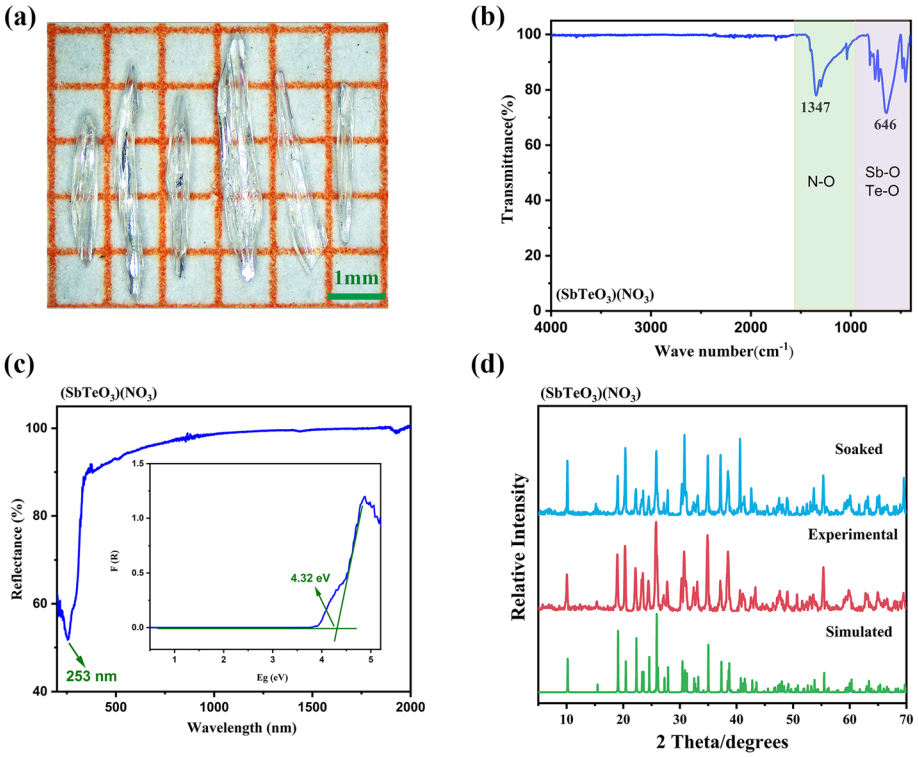

Fig. 2 As grown crystals (a), infrared spectrum (b), and UV-vis-NIR diffuse-reflectance spectrum (c) of $(SbTeO_3)(NO_3)$ (c); simulated, experimental, and soaked PXRD pattern for $(SbTeO_3)(NO_3)$ (d).

while the O–Sb–O angles are about 4.5° smaller than those of O–Te–O (Fig. 1a and Table S3†). The N–O bonds and O–N–O angles are in the ranges of 1.238(7)–1.275(7) Å and 119.2(5)–121.1(5)°, respectively (Fig. 1a and Table S3†). The calculated bond valence sums for Sb, Te, and N are 2.879, 3.667, and 4.818, signifying their oxidation states as +3, +4, and +5, respectively (Tables S3 and S4†).

$(SbTeO_3)(NO_3)$ presents a sandwich-type two-dimensional (2D) layered structure (Fig. 1b). The triangular pyramids, $[SbO_3]$ and $[TeO_3]$, were interconnected into a 2D $[SbTeO_3]^+$ cationic layer parallel to the *ac* plane *via* corner-sharing with $[Sb_3Te_3]$ 6-member polyhedral rings (MPRs) (Fig. 1c and S3†). The SCALP (stereochemically active lone pair) electrons on the $[SbO_3]$ and $[TeO_3]$ units point towards the interlayer gaps, reducing the repulsion of lone-pairs and enhancing the stability of the overall structure. The distance between adjacent cationic layers corresponds to the length of the crystallographic *b*-axis, approximately 8.66 Å (Fig. 1b). The isolated $[NO_3]^-$ planar triangles were filled between the 2D cationic layers to maintain the charge balance. In addition to the electric field force from positive and negative charges, there are weak Te–O bonds (2.549 Å) between the nitrates and tellurites (Fig. S4†).

Based on the geometric structure of $(SbTeO_3)(NO_3)$, dipole moment calculations were employed to evaluate the spatial arrangement of the three NLO-active groups (Table S5†). The local dipole moments of the $[SbO_3]$, $[TeO_3]$, and $[NO_3]$ units were calculated to be 28.840, 6.884, and 0.548 D, respectively. From Table S5,† we can find that the dipole moments of $(SbTeO_3)(NO_3)$ in the *x*- and *y*-components were fully cancelled, while those in the *z*-component were effectively added. As shown in Fig. 1d, despite the large dihedral angle (72.056°) between the trigonal planes, the nitrate groups still exhibit polarity in the *c*-axis direction. The net dipole moment of $(SbTeO_3)(NO_3)$ was calculated to be 36.272 D. The dipole moment per unit cell is 0.069 D $Å^{-3}$, which surpasses those of $CsVO_2F(IO_3)$ (0.05 D $Å^{-3}$),[33] $RbGa_3F_6(SeO_3)_2$ (0.01 D $Å^{-3}$),[34] and *α*- and β-$Ba_2GaF_4(IO_3)_2$ (0.044 and 0.043 D $Å^{-3}$).[35]

The thermogravimetric analysis (TGA) of $(SbTeO_3)(NO_3)$ was conducted in a nitrogen atmosphere within a temperature range of 20–1200 °C (Fig. S5†). The TG curve encompasses three steps of weight loss. The first one (exp. 4.37%) in the range of 273 °C to 366 °C was in accordance with the release of 0.5 molecules of O_2 (cal. 4.45%). The second weight loss (exp. 8.26%) occurred above 639 °C and can be attributed to the evaporation of 1 molecule of NO (cal. 8.35%).[36] Finally, upon heating to 825 °C, TeO_2 and Sb_2O_3 began to escape.[37] The residue above 1000 °C was checked using PXRD to determine its phase. By comparison, it was found that the main components of the residue were Sb_2O_4 and small amounts of unknown amorphous compounds (Fig. S6†).

The IR spectrum of $(SbTeO_3)(NO_3)$ was measured in the wavenumber range of 4000 to 400 cm^{-1}. As shown in Fig. 2b, the absorption bands and peaks of N–O, Te–O and Sb–O vibrations appeared. The stretching vibrations of N–O bonds occur at around 1347 cm^{-1}. The absorption peaks around 646 cm^{-1} can be attributed to the vibrations of Te–O and Sb–O bonds. These

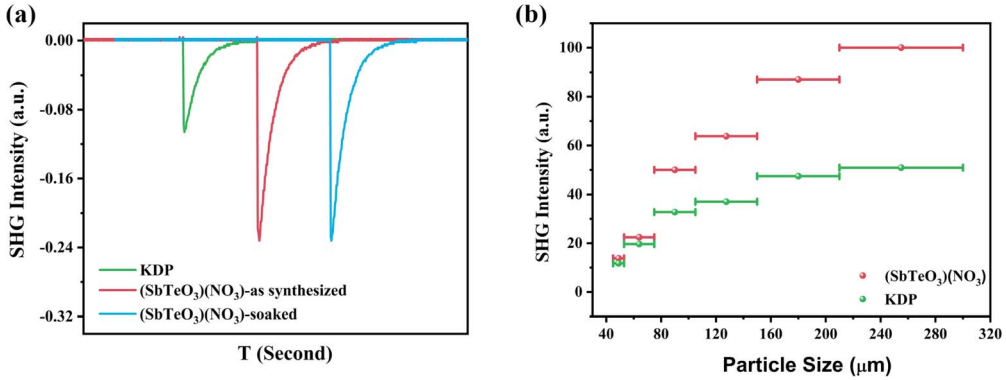

Fig. 3 Oscilloscope traces of SHG signals for as-synthesized $(SbTeO_3)(NO_3)$ and $(SbTeO_3)(NO_3)$ soaked in deionized water for 30 days in the particle size range of 150–210 μm (KDP sieved in the same particle sizes was used as a reference) (a), and SHG intensity *versus* particle size curves at 1064 nm for $(SbTeO_3)(NO_3)$ (b).

assignments align with those reported in previously studied compounds.[38–40]

The UV-vis-NIR diffuse-reflectance spectrum revealed that $(SbTeO_3)(NO_3)$ is transparent in the ultraviolet to near-IR range (Fig. 2c). Its UV cutoff edge was measured to be 253 nm, corresponding to a bandgap of 4.32 eV (Fig. 2c), which is larger than those of the reported nitrate tellurite NLO crystals, such as $Bi_3(\mu_3\text{-}OH)(TeO_3)_3(NO_3)_2$ (3.3 eV)[41] and $Bi_2Te_2O_6(NO_3)_2(OH)_2(H_2O)$ (4.0 eV)[42] (Table S6†).

The powder SHG intensities of $(SbTeO_3)(NO_3)$ and KH_2PO_4 (KDP) (as a reference) were measured using a 1064 nm Q-switch laser based on the Kurtz–Perry method. $(SbTeO_3)(NO_3)$ displays a large SHG signal of 2.2 times that of KDP in the particle size range of 150–210 μm under 1064 nm laser radiation (Fig. 3a). As shown in Fig. 3b, the SHG signal increases upon increasing the particle size from 45 to 300 μm, indicating that $(SbTeO_3)(NO_3)$ can realize phase-matching. Compared with the reported tellurite nitrates, antimonite nitrates and antimonite tellurites,[36,38,41–48] the title compound features the optimally balanced performance (Fig. 4). $(SbTeO_3)(NO_3)$ is the only compound with SHG intensity larger than 2 × KDP and E_g higher than 4.2 eV in these systems (Table S6†). This result underscores the effectiveness of the fully tricoordinated assembly strategy.

$(SbTeO_3)(NO_3)$ displays a high laser-induced damage threshold (LIDT) of 139.19 MW cm^{-2}, which is much larger than that of $In_2(SO_4)(TeO_3)(OH)_2(H_2O)$ (79.6 MW cm^{-2})[49] and comparable with those of $PbCdF(NO_3)(SeO_3)$ (135.6 MW cm^{-2})[29] and $Cs_6Sb_4Mo_3O_5F_{26}$ (133.5 MW cm^{-2}).[50] The high LIDT of $(SbTeO_3)(NO_3)$ can be attributed to its large band gap and the strong N–O covalent bonds.

In addition to excellent linear and nonlinear optical properties, chemical stability, especially water resistance, is crucial for the practical application of NLO crystals. Nitrates are excellent candidate materials for UV NLO, but they have long been faced with a significant challenge of poor water resistance. For example, the $K_2RE(NO_3)_5\cdot 2H_2O$ (RE = La, Ce, Pr, or Nd) series of compounds exhibit a strong SHG effect, approximately three times that of KDP, but they are extremely deliquescent.[51]

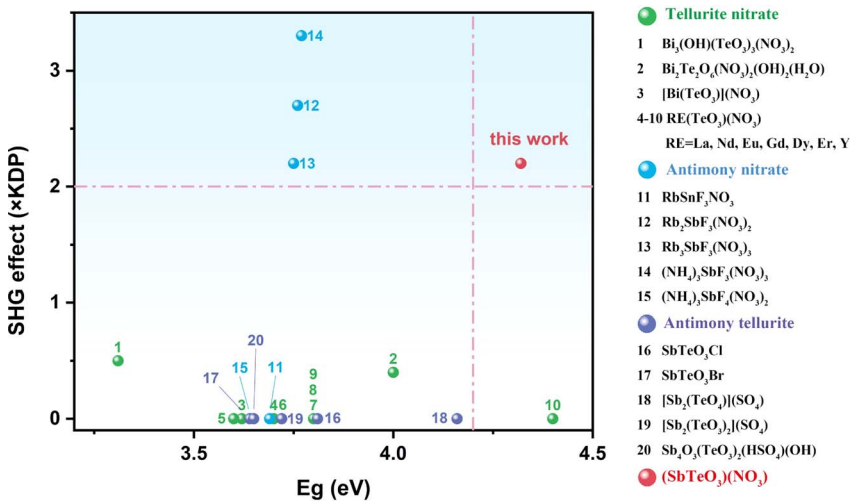

Fig. 4 Performance comparison of tellurite nitrate, antimony nitrate and antimony tellurite families.

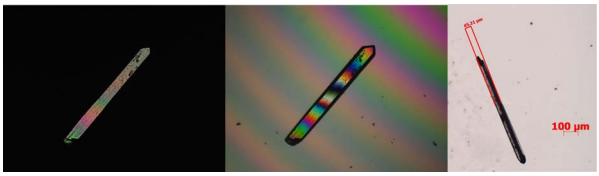

Fig. 5 An $(SbTeO_3)(NO_3)$ crystal under a polarizing microscope: before the optical path compensation, after compensation, and thickness.

To evaluate the water resistance of $(SbTeO_3)(NO_3)$, we submerged crystals weighing 93.9 mg in 50 mL of deionized water at room temperature for 30 days. Surprisingly, the crystals remained unchanged in weight and transparency, indicating their chemical stability and insolubility in water. The PXRD pattern of the soaked sample matches with those of both simulated and unsoaked crystals (Fig. 2d), further attesting to its stability. Additionally, the SHG effect of particles with diameters between 150 and 210 μm showed no significant variation after soaking for 30 days, as depicted in Fig. 3a, underscoring the high water resistance of $(SbTeO_3)(NO_3)$ and its potential as an exceptional NLO material.

We analysed the possible mechanism of high water resistance of $(SbTeO_3)(NO_3)$ from the perspective of its crystal chemical structure. (i) According to the principle of "like dissolves like", water-resistant nitrates should exhibit structures akin to insoluble compounds, differing in polarity from water molecules.[14] $(SbTeO_3)(NO_3)$ exhibits a layered structure similar to that of layered double hydroxides (LDHs) (Fig. S7†), which is not easily soluble in water, as observed previously in water-resistant compounds such as $Ba_2NO_3(OH)_3$ [52] and $Bi_3TeO_6OH(NO_3)_2$.[53] (ii) In nitrates where $[NO_3]^-$ coordinates with other cations,[54] such as $A_2RE(NO_3)_5\cdot 4H_2O$ (A^+ = Rb^+ or NH_4^+)[55,56], the presence of delocalized π-bonds within $[NO_3]^-$ weakens its coordination with the cations, making the lattice more susceptible to disruption and dissolution in aqueous environments. However, in $(SbTeO_3)(NO_3)$, $[NO_3]^-$ units are isolated, preventing lattice disruption by H_2O. (iii) The SCALP electrons on Sb^{3+} and Te^{4+} are oriented towards the interlayer $[NO_3]^-$ groups, creating significant steric hindrance, which to some extent can prevent the $[NO_3]^-$ groups between the layers from forming hydrogen bonds with external water molecules, limiting the interaction between $[NO_3]^-$ and water molecules and discouraging the dissolution process. For example, nitrates with SCALP electrons, such as $[Bi_6O_4(OH)_4](NO_3)_6\cdot 4H_2O$[57] and $Pb_2(NO_3)_2(H_2O)F_2$,[58] all exhibit good water resistance. (iv) Significant repulsion occurs between the lone pairs of electrons on Sb^{3+} and Te^{4+} and the lone pairs on O^{2-} in external H_2O, thereby reducing its solubility in water. Consequently, the exceptional water resistance of $(SbTeO_3)(NO_3)$ is attributed to the fully tricoordinated assembly strategy of gradually lowering

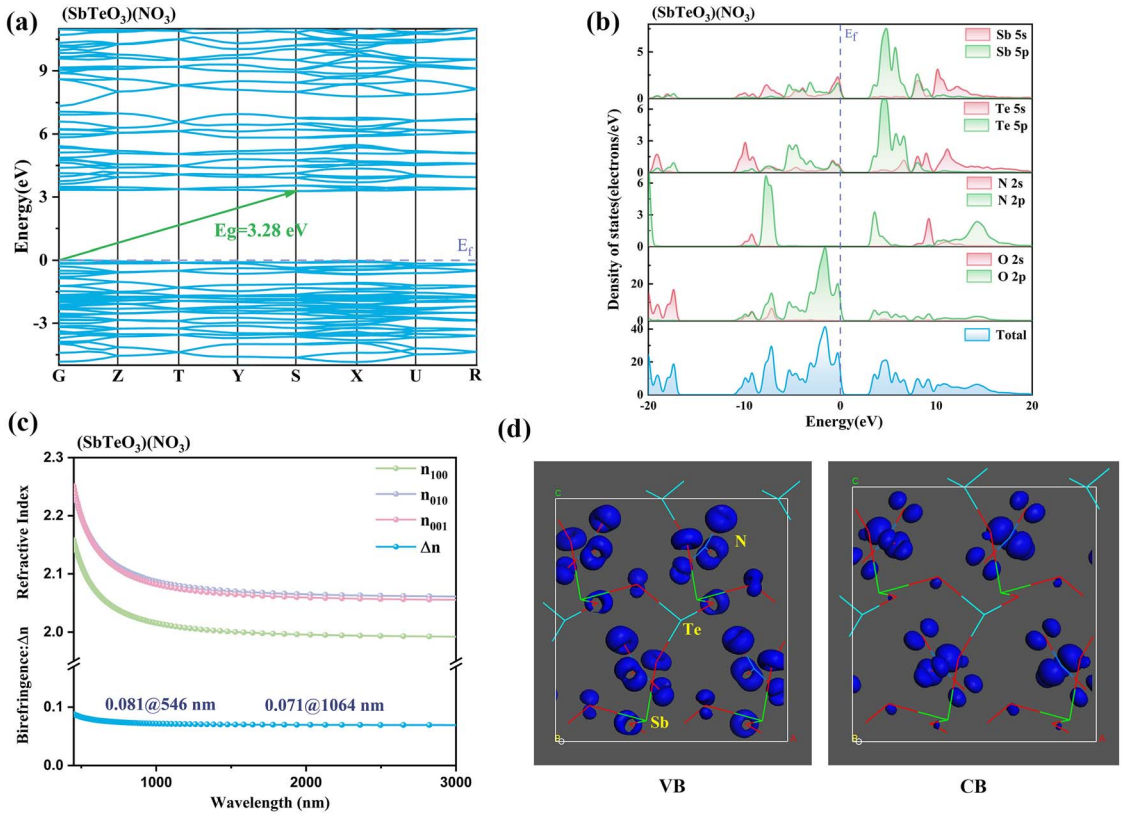

Fig. 6 The calculated band structure (a), total and partial density of states (b), and calculated refractive index dispersion and birefringence curves (c) of $(SbTeO_3)(NO_3)$, and the SHG-weighted electron density for the VB and CB in $(SbTeO_3)(NO_3)$ (d).

the valence state of the central cations. According to Pauling's rules, the [NO_3] groups with high valency tend to be isolated, which is the main reason for the layered structure of ($SbTeO_3$)(NO_3).

The birefringence of ($SbTeO_3$)(NO_3) was measured using a polarizing microscope. Its optical path difference is 3.515 μm, and the single crystal thickness is 45.21 μm (Fig. 5). According to the formula $\Delta n = R/T$ (where R stands for the optical path difference and T represents the thickness), the experimental birefringence of ($SbTeO_3$)(NO_3) at $\lambda = 546$ nm is found to be 0.078, which is approximately in line with the calculated birefringence value (0.081 at 546 nm).

To elucidate the intrinsic structure–property relationship of ($SbTeO_3$)(NO_3), we conducted systematic theoretical calculations using density functional theory (DFT). As shown in Fig. 6a, the theoretical bandgap of ($SbTeO_3$)(NO_3) is 3.28 eV. The total density of states (DOS) and partial density of states (PDOS) for each element in ($SbTeO_3$)(NO_3) are depicted in Fig. 6b, revealing several electronic characteristics: (i) strong hybridization between the 5s and 5p orbitals of Sb, Te, N, and O within the −11 to 0 eV and 0 to 15 eV range, indicating strong covalent interactions within the [SbO_3], [TeO_3], and [NO_3] moieties, (ii) the valence band (VB) top from −5 to 0 eV is primarily occupied by non-bonding orbitals of O-2p, while the conduction band (CB) bottom from 0 to 5 eV is mainly contributed by N-2p, O-2p, Te-5p and Sb-5p orbitals. Optical properties hinge on transitions near the Fermi level, governed by [SbO_3], [TeO_3], and [NO_3] units. Calculated birefringence values of 0.081@546 nm and 0.071@1064 nm (Fig. 6c) facilitate SHG phase matching.

To further delineate the SHG effect of ($SbTeO_3$)(NO_3), its SHG coefficient and SHG-weighted density were calculated. Crystallized in the $Pca2_1$ space group (point group: $mm2$), ($SbTeO_3$)(NO_3) has three non-zero independent SHG coefficients under Kleinman symmetry restrictions: $d_{31} = d_{15} = -0.87725$ pm V^{-1}, $d_{32} = d_{24} = -1.0845$ pm V^{-1} and $d_{33} = 4.632$ pm V^{-1}. Among these, the maximum calculated SHG coefficient is d_{33}, and the effective SHG coefficient (d_{eff}) is calculated to be 1.95 pm V^{-1}, which exceeds that of many NLO crystals, such as $Sc(IO_3)_2(NO_3)$ ($d_{11} = d_{22} = 1.49$ pm V^{-1}),[59] $La(IO_3)_2(NO_3)$ ($d_{16} = d_{21} = 0.703$ pm V^{-1}),[60] $Bi_3TeO_6OH(NO_3)_2$ ($d_{16} = -1.31$ pm V^{-1}),[53] $La(OH)_2NO_3$, $Gd(OH)_2NO_3$ and $Y(OH)_2NO_3$ ($d_{eff} = 1.396$, 1.464 and 1.478 pm V^{-1}),[61] and $Rb_2SbFP_2O_7$ ($d_{24} = 0.63$ pm V^{-1}).[62]

In the virtual electron processes, SHG-weighted electron clouds of ($SbTeO_3$)(NO_3) predominantly localize on the tricoordinated NLO-active groups [NO_3], [SbO_3], and [TeO_3]. For the VB, SHG-weighted electron density is localized on the non-bonding O-2p orbitals, whereas for the CB, the π* antibonding orbitals of the [NO_3] moiety contribute significantly to the SHG response (Fig. 6d). Additionally, the SHG contribution values for the [SbO_3], [TeO_3], and [NO_3] units are 20.92%, 23.88%, and 55.12%, respectively. This indicates that the strong SHG effect of ($SbTeO_3$)(NO_3) stems from the synergistic interaction of the three tricoordinated NLO-active moieties, highlighting the intrinsic origin of the efficacy of the fully tricoordinated NLO-active moiety assembly strategy.

Conclusions

In summary, based on the fully tricoordinated assembly strategy, the first antimony tellurite NLO crystal, ($SbTeO_3$)(NO_3), has been obtained at room temperature through a facile evaporation method. ($SbTeO_3$)(NO_3) stands out among all tellurite, antimonite nitrate and antimonite-tellurite families for the optimally balanced properties: a short UV cutoff edge (253 nm), strong phase-matched SHG intensity (2.2 × KDP), moderate birefringence (0.081@546 nm), exceptional water resistance (30 days) and large crystals (>4 mm). First-principles calculations revealed that the maximum SHG coefficient d_{33} of ($SbTeO_3$)(NO_3) is 4.63 pm V^{-1}, with an effective coefficient (d_{eff}) of 1.95 pm V^{-1}, outperforming the majority of tellurite and antimony nitrates. The theoretical calculations confirmed the synergistic effect of the three functional groups and the SHG contributions of the [SbO_3], [TeO_3], and [NO_3] units are 20.92%, 23.88%, and 55.12%, respectively. The fully tricoordinated assembly strategy also has a positive effect on enhancing the physical and chemical stability of nitrates. The unique LDH structure with two types of SCALP electrons enables ($SbTeO_3$)(NO_3) to effectively overcome the poor water resistance inherent in nitrates. This work not only fills a gap in the research into antimony tellurite NLO crystals but also underscores the potential of the fully tricoordinated assembly strategy in materials science, offering new avenues for the development of advanced optical materials.

Data availability

The data supporting this article have been included as part of the ESI.† Crystallographic data for ($SbTeO_3$)(NO_3) has been deposited at the CCDC under 2259072 and can be obtained from **https://www.ccdc.cam.ac.uk/structures**.

Author contributions

Bo Zhang: investigation, formal analysis, writing – original draft. Chun-Li Hu: theoretical calculations. Jiang-Gao Mao: supervision, funding acquisition. Fang Kong: conceptualization, project administration, writing – review & editing. All authors have given approval to the final version of the manuscript.

Conflicts of interest

There are no conflicts to declare.

Acknowledgements

This work was supported by the National Natural Science Foundation of China (Grant No.: 22475215, 22031009, 22375201 and 21921001), the NSF of Fujian Province (Grant No.: 2023J01216) and the Self-deployment Project Research Program of Haixi Institutes, Chinese Academy of Sciences (CXZX-2022-GH06).

Notes and references

1 M. Mutailipu, J. Han, Z. Li, F. M. Li, J. Li, F. F. Zhang, X. F. Long, Z. H. Yang and S. L. Pan, *Nat. Photonics*, 2023, **17**, 694–701.

2 K. C. Chen, C. S. Lin, G. Peng, Y. Chen, H. Z. Huang, E. Z. Chen, Y. X. Min, T. Yan, M. Luo and N. Ye, *Chem. Mater.*, 2022, **34**, 399–404.

3 X. F. Wang, X. D. Leng, Y. Kuk, J. Lee, Q. Jing and K. M. Ok, *Angew. Chem., Int. Ed.*, 2023, **136**, e202315434.

4 W. Zhou and S. P. Guo, *Acc. Chem. Res.*, 2024, **57**, 648–660.

5 L. Chen, Z. P. Zhang, X. Liu, R. X. Wang, S. Zhao, W. J. He, H. Y. Chen, X. B. Deng, L. M. Wu and Z. Y. Zhou, *Angew. Chem., Int. Ed.*, 2024, e202408551.

6 J. J. Zhou, H. P. Wu, H. W. Yu, S. T. Jiang, Z. G. Hu, J. Y. Wang, Y. C. Wu and P. S. Halasyamani, *J. Am. Chem. Soc.*, 2020, **142**, 4616–4620.

7 L. Wu, C. Lin, H. Tian, Y. Zhou, H. Fan, S. Yang, N. Ye and M. Luo, *Angew. Chem., Int. Ed.*, 2023, **63**, e202315647.

8 M. Y. Ran, S. H. Zhou, W. B. Wei, B. X. Li, X. T. Wu, H. Lin and Q. L. Zhu, *Small*, 2023, **20**, 2304563.

9 H. Liu, H. Wu, Z. Hu, J. Wang, Y. Wu and H. Yu, *J. Am. Chem. Soc.*, 2023, **145**, 12691–12700.

10 L. Wang, D. Chu, Z. Yang, J. Li and S. Pan, *Chem. Sci.*, 2024, **15**, 6577–6582.

11 P. F. Li, C. L. Hu, J. G. Mao and F. Kong, *Chem. Sci.*, 2024, **15**, 7104–7110.

12 B. W. Liu, X. M. Jiang, S. M. Pei, W. F. Chen, L. Q. Yang and G. C. Guo, *Mater. Horiz.*, 2021, **8**, 3394–3398.

13 H. Wu, Z. Wei, Z. Hu, J. Wang, Y. Wu and H. Yu, *Angew. Chem., Int. Ed.*, 2024, **63**, e202406318.

14 X. Liu, P. Gong, Y. Yang, G. Song and Z. Lin, *Coord. Chem. Rev.*, 2019, **400**, 213045.

15 F. Hou, D. Mei, M. Xia and Y. Wu, *Coord. Chem. Rev.*, 2021, **444**, 214038.

16 P. F. Li, C. L. Hu, B. X. Li, J. G. Mao and F. Kong, *Inorg. Chem.*, 2024, **63**, 4011–4016.

17 X. P. Shi, A. Tudi, M. Gai, Z. H. Yang, S. J. Han and S. L. Pan, *Chem. Mater.*, 2023, **35**, 5680–5688.

18 D. Dou, Q. Shi, H. Li, B. Zhang, D. Yang and Y. Wang, *Adv. Sci.*, 2024, **11**, 2401325.

19 M. Mutailipu, K. R. Poeppelmeier and S. L. Pan, *Chem. Rev.*, 2021, **121**, 1130–1202.

20 H. T. Qiu, F. M. Li, Z. Li, Z. H. Yang, S. L. Pan and M. Mutailipu, *J. Am. Chem. Soc.*, 2023, **145**, 24401–24407.

21 X. M. Liu, L. Kang, P. F. Gong and Z. S. Lin, *Angew. Chem., Int. Ed.*, 2021, **60**, 13574–13578.

22 C. Wu, L. Lin, T. H. Wu, Z. P. Huang and C. Zhang, *J. Solid State Chem.*, 2021, **298**, 122095.

23 M. L. Liang, Y. X. Ma, C. L. Hu, F. Kong and J. G. Mao, *Chem. Mater.*, 2020, **32**, 9688–9695.

24 Q. Wang, X. H. Dong, L. Huang, K. M. Ok, Z. E. Lin and G. H. Zou, *Small*, 2023, **19**, e2302797.

25 Q. Q. Chen, C. L. Hu, J. Chen, Y. L. Li, B. X. Li and J. G. Mao, *Angew.Chem., Int. Ed.*, 2021, **60**, 17426–17429.

26 Q. Wu, J. F. Zhou, X. M. Liu, X. Jiang, Q. Zhang, Z. Lin and M. J. Xia, *Inorg. Chem.*, 2021, **60**, 18512–18520.

27 P. F. Li, C. L. Hu, J. G. Mao and F. Kong, *Coord. Chem. Rev.*, 2024, **517**, 216000.

28 G. Peng, C. Lin, H. Fan, K. Chen, B. Li, G. Zhang and N. Ye, *Angew. Chem., Int. Ed.*, 2021, **60**, 17415–17418.

29 Y. X. Ma, C. L. Hu, B. X. Li, F. Kong and J. G. Mao, *Inorg. Chem.*, 2018, **57**, 11839–11846.

30 J. L. Song, C. L. Hu, X. Xu, F. Kong and J. G. Mao, *Angew. Chem., Int. Ed.*, 2015, **54**, 3679–3682.

31 Y. Liu, X. Liu, S. Liu, Q. Ding, Y. Li, L. Li, S. Zhao, Z. Lin, J. Luo and M. Hong, *Angew. Chem., Int. Ed.*, 2020, **59**, 7793–7796.

32 F. Kong, S. P. Huang, Z. M. Sun, J. G. Mao and W. D. Cheng, *J. Am. Chem. Soc.*, 2006, **128**, 7750–7751.

33 J. Chen, C. L. Hu, X. H. Zhang, B. X. Li, B. P. Yang and J. G. Mao, *Angew. Chem., Int. Ed.*, 2020, **59**, 5381–5384.

34 C. Wu, X. X. Jiang, L. Lin, Z. S. Lin, Z. P. Huang, M. G. Humphrey and C. Zhang, *Chem. Mater.*, 2020, **32**, 6906–6915.

35 H. Yu, M. L. Nisbet and K. R. Poeppelmeier, *J. Am. Chem. Soc.*, 2018, **140**, 8868–8876.

36 C. Y. Meng, M. F. Wei, L. Geng, P. Q. Hu, M. X. Yu and W. D. Cheng, *J. Solid State Chem.*, 2016, **239**, 46–52.

37 T. Zhang, J. Jiao, W. Zhao, F. Wang, F. Liang, N. Ye, Z. Hu, Y. Wu and C. Li, *Inorg. Chem.*, 2023, **62**, 17522–17529.

38 Q. Wang, J. X. Ren, D. Wang, L. L. Cao, X. H. Dong, L. Huang, D. J. Gao and G. H. Zou, *Inorg. Chem. Front.*, 2023, **10**, 2107–2114.

39 B. Zhang, J. H. Wu, C. L. Hu, Y. F. Li, F. Kong and J. G. Mao, *Inorg. Chem. Front.*, 2023, **10**, 1328–1337.

40 Y. L. Lv, W. Xu, W. D. Yao, M. B. Xu, W. Liu, S. P. Guo and R. L. Tang, *Inorg. Chem.*, 2024, **63**, 6127–6131.

41 J. L. Song and C. Qian, *ChemistrySelect*, 2017, **2**, 1681–1685.

42 S. Lee, H. Jo and K. M. Ok, *J. Solid State Chem.*, 2019, **271**, 298–302.

43 H. E. Lee, H. Jo, M. H. Lee and K. M. Ok, *J. Alloys Compd.*, 2021, **851**, 156855.

44 L. Wang, H. m. Wang, D. Zhang, D. j. Gao, J. Bi, L. Huang and G. h. Zou, *Inorg. Chem. Front.*, 2021, **8**, 3317–3324.

45 L. Wang, F. Yang, X. Y. Zhao, L. Huang, D. J. Gao, J. Bi, X. Wang and G. H. Zou, *Dalton Trans.*, 2019, **48**, 15144–15150.

46 X. Y. Zhou, X. Mao, P. Zhang, X. H. Dong, L. Huang, L. L. Cao, D. J. Gao and G. H. Zou, *Inorg. Chem. Front.*, 2024, **11**, 3221–3228.

47 J. Y. Zhang, X. Zhao, Y. D. Wu, D. J. Mei, S. G. Wen and T. Doert, *Z. Anorg. Allg. Chem.*, 2021, **647**, 1269–1276.

48 X. F. Li, K. Wang, C. He, J. H. Li, X. T. An, J. Pan, Q. Wei, G. M. Wang and G. Y. Yang, *Inorg. Chem.*, 2023, **62**, 7123–7129.

49 Y. P. Gong, Y. X. Ma, S. M. Ying, J. G. Mao and F. Kong, *Inorg. Chem.*, 2019, **58**, 11155–11163.

50 J. H. Wu, B. Zhang, T. K. Jiang, F. Kong and J. G. Mao, *Chin. J. Struct. Chem.*, 2023, **42**, 100016.

51 W. T. Dong, H. J. Zhang, Q. Su, Y. H. Lin, S. M. Wang and C. S. Zhu, *J. Solid State Chem.*, 1999, **148**, 302–307.

52 X. Dong, L. Huang, Q. Liu, H. Zeng, Z. Lin, D. Xu and G. Zou, *Chem. Commun.*, 2018, **54**, 5792–5795.
53 S. G. Zhao, Y. Yang, Y. G. Shen, B. Q. Zhao, L. N. Li, C. M. Ji, Z. Y. Wu, D. Q. Yuan, Z. S. Lin, M. C. Hong and J. H. Luo, *Angew. Chem., Int. Ed.*, 2017, **56**, 540–544.
54 I. V. Morozov, V. N. Serezhkin and S. I. Troyanov, *Russ. Chem. Bull.*, 2008, **57**, 439–450.
55 L. Bohatý, P. Held, P. Becker and Z. Anorg, *Allg. Chem.*, 2009, **635**, 2236–2241.
56 L. Bohatý, R. Fröhlich, P. Held and P. Becker, *Eur. J. Inorg. Chem.*, 2010, **2010**, 2642–2648.
57 N. Henry, O. Mentré, F. Abraham, E. J. MacLean and P. Roussel, *J. Solid State Chem.*, 2006, **179**, 3087–3094.
58 G. Peng, Y. Yang, Y.-H. Tang, M. Luo, T. Yan, Y. Zhou, C. Lin, Z. Lin and N. Ye, *Chem. Commun.*, 2017, **53**, 9398–9401.
59 C. Wu, X. Jiang, Z. Wang, L. Lin, Z. Lin, Z. Huang, X. Long, M. G. Humphrey and C. Zhang, *Angew. Chem., Int. Ed.*, 2021, **60**, 3464–3468.
60 F. F. Mao, C. L. Hu, B. X. Li and J. G. Mao, *Inorg. Chem.*, 2017, **56**, 14357–14365.
61 Y. Song, M. Luo, C. Lin and N. Ye, *Chem. Mater.*, 2017, **29**, 896–903.
62 X. Dong, H. Huang, L. Huang, Y. Zhou, B. Zhang, H. Zeng, Z. Lin and G. Zou, *Angew. Chem., Int. Ed.*, 2024, **63**, e202318976.